

DESIGN AND IMPLEMENT OF A CONICAL AIRBORNE LIDAR SCANNING SYSTEM

Haocheng Hu^{1,2}, Guoqing Zhou^{1,2,3} Xiang Zhou^{1,2,3,*}, Yizhi Tan^{1,2}, Jiandong Wei^{1,2}

¹ College of Mechanical and Control Engineering, Guilin University of Technology, No. 12 Jian'gan Road, Guilin, Guangxi 541004, China

² Guangxi Key Laboratory of Spatial Information and Geomatics, Guilin University of Technology, No. 12 Jian'gan Road, Guilin, Guangxi 541004, China

³ School of Microelectronics, Tianjin University, No. 92 Weijin Road, Tianjin 300072, China

KEY WORDS: Airborne LiDAR, Conical Scanning System, Optical system, Refracting prism

ABSTRACT:

At present, the main LiDAR is single-point lidar. APD arrays and laser arrays are restricted to exit, so the number of area array LiDAR is scarce. Single-point lidar can't form a scanning pattern with only one laser point on the ground after launching laser, so it must have a set of scanning device for single-point lidar. The scanning device designed in this paper forms a circular scanning area on the ground by rotating the refraction prism, and at the same time forms a conical field of view. At present, marine LiDAR uses this kind of scanner more frequently. The advantages of this scanner are: simple mechanical structure and smooth operation. Overlapping elliptical scanning trajectories can be obtained during flight, which increases scanning density. Ultra-low dispersion glass is used as refractive prism in this paper. In a certain range of laser frequencies, the refractive prism has almost the same effect on laser refraction at different frequencies. The simulation results show that the scanner can be used as a common LiDAR scanner or a dual-frequency LiDAR scanner.

* Correspondence author, E-mail: zqx0711@glut.edu.cn

1. INTRODUCTION

Airborne LiDAR is a new technology for measuring spatial information, which can directly obtain the distance observation value. The DEM produced by airborne LiDAR is faster than aerial photogrammetry. It can be used in forestry, traffic surveying, strip target topographic mapping, urban three-dimensional modeling and so on (Wang, 2013). Area array LiDAR has multi-point laser source, but area array laser source and APD array are expensive and prohibited by many countries. At present, single laser point LiDAR is mainly used. A complete scanning system structure includes laser, laser collimation beam expanding system, optical wedge, hollow rotary motor and sensor of detection motor. Pulsed laser sources can be divided into gas lasers, solid-state lasers, semiconductor lasers, fiber lasers and other concentrated types. Semiconductor lasers have the advantages of high conversion efficiency, small size, high reliability, direct debugging and easy to be reproduced on small aircraft (G. Kamoske, 2019). And so on. In this paper, a 1064-nm semiconductor laser is used.

Our team got a project called ‘Land and Sea Dual Frequency LiDAR’ in Guangxi. The LiDAR developed by the project needs to be able to map both land and shallow water. Figure 1 is a schematic diagram of Lidar. About this project, this paper design a kind of scanning device.

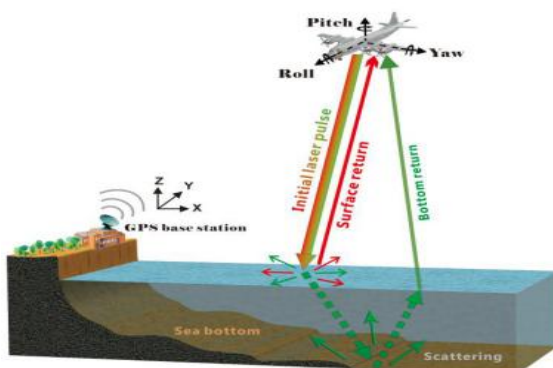


Figure 1. Dual LiDAR working diagram

2. BASIC THORY OF LIDAR SCANNING DEVICE

Laser emitter can only emit one laser point at a time. In order to form scanning pattern for scanning point in flight, it is necessary to cooperate with scanning device. At present, there are three typical mechanical scanning modes in the scanner. Pendulum scanning, rotating polyhedron, rotating regular polyhedron.

2.1 Scanning device of pendulum mirror

Pendulum scanning is the most mature scanning mode at present, which is adopted by many advanced LiDAR systems. The schematic diagram is shown in Figure 2. The system drives the mirror to rotate by an electric motor. When the mirror is in different positions, the angle between the incident light and the mirror surface changes periodically, and the corresponding reflected light emits at different angles. So, the laser point will move periodically on the ground to form a scanning pattern.

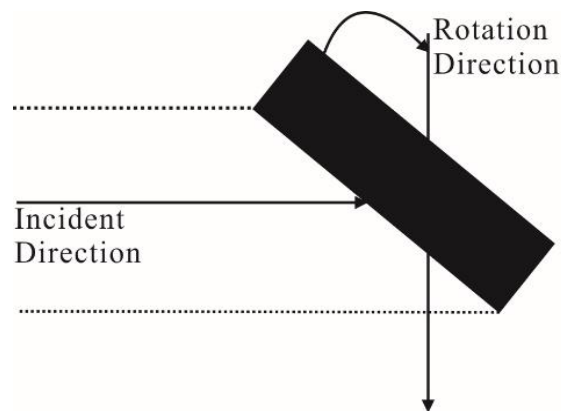


Figure 2. Principle of Pendulum Scanning Device

2.2 Scanning device of rotating polyhedron

Rotating polyhedral mirror is not often used in mainstream lidar, and it is widely used in marine LiDAR. It is the type of LiDAR scanner used in this paper. Use a reflecting mirror or prism with a rotating axis. When the laser irradiates the mirror surface, the ground will form an ellipse with every rotation of the mirror. With the flight of an aircraft, numerous ellipses are formed in the direction of flight.

2.3 Scanning device for rotating regular polyhedron

Rotating regular polyhedron scanning is a common scanning method. Many commercial LiDAR systems adopt this approach. The regular polyhedron is used as a reflection prism, and the motor drives the rotation to make the polyhedron prism rotate at a uniform speed. With the change of incident angle, the reflected beam also changes. Scanning patterns are formed on the ground. The scanning pattern formed by this kind of device is a straight line with equal spacing. Scanning points are evenly distributed. The schematic diagram is shown in Figure 3.

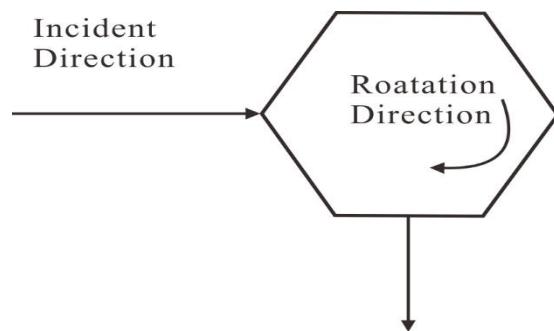


Figure 3. Principle Diagram of Rotating Polyhedron Device

3 ARDWARE SYSTEM DESIGN

3.1 Scanning System Index

This scanning system has the following features

- (1) Possessing certain detection capability of sea surface and land.
- (2) Have the ability of laser circular scanning.
- (3) It has large aperture and has certain universality for other wavelength lasers.

Indicators such as Table 1

Aircraft flight altitude	h (m)
Half scan angle	θ (rad)
Control motor speed	n (circle/s)
Aircraft Flight Speed	v (m/s)
Time elapsed from zero	t (s)
Scanning radius	R (m)
Laser Pulse Interval	t_0 (s)

Table 1. Scanner Index Parameters Table

3.2 Dynamic Scanning Corner Model

Definitions of various mathematical quantities are shown in Table 2

This paper only establishes a simple standard dynamic mathematical model, and the actual situation also needs to consider the factors such as aircraft attitude.

parameter	data
Wedge diameter	200mm
Laser damage threshold	>2J/cm ²
Laser wavelength	1064nm、532nm
Laser Scanning Corner Points	176
Scan width	350m
Scanning grid point density	4×4
Aircraft speed range	200km/h--270km/h
Laser frequency	5.5kHz

Table 2. Mathematical Quantity Definition Table

In order to facilitate calculation, the mathematical model is described. All motion occurs in the first quadrant of the coordinate system. The aircraft starts flying from (R, 0) and the initial turning of the motor chooses the counterclockwise direction. At zero time, the laser scanning corner position is (0,0). Then, every t_0 time, the laser emits pulses again.

The position model of scanning corner is described, and the scatter plot of MATLAB is further studied. In order to simplify the problem, zero-time and T-Time can be selected to study. The position of the two scanning corners passes through t . The flight distance of the aircraft is vt , so the distance between the two centers is vt . $R = htan \theta$ is obtained from the triangular relation. Because of the rotation of the motor, the final additional advance distance at the laser point is $Rsin_t$, which is brought in to get $htan \theta sin_t$. The additive result is the longitudinal coordinate formula of scatter points. (possibly because the angle is larger than pi, the result is smaller than vt)

$$y = vt + htan\theta sin\omega t \quad (1)$$

The range of abscissa values is only possible in the range of (0, 2R). From the triangle relationship. The abscissa formula can be obtained.

$$x = htan\theta - htan\theta cos\omega t \quad (2)$$

Formula for the Relation between Angular Speed and Rotating Speed

$$\omega = 2\pi n \quad (3)$$

The final expression is

$$\begin{cases} y = vt + htan\theta sin(2\pi nt) \\ x = htan\theta - htan\theta cos(2\pi nt) \end{cases} \quad (4)$$

The simulation results are shown in Fig4. After 6 seconds scanning, an elliptical scanning area is formed on the ground. Based on the image, it is reasonable to estimate the rotation rate of the scanning motor between 1800 rpm and 1900 rpm.

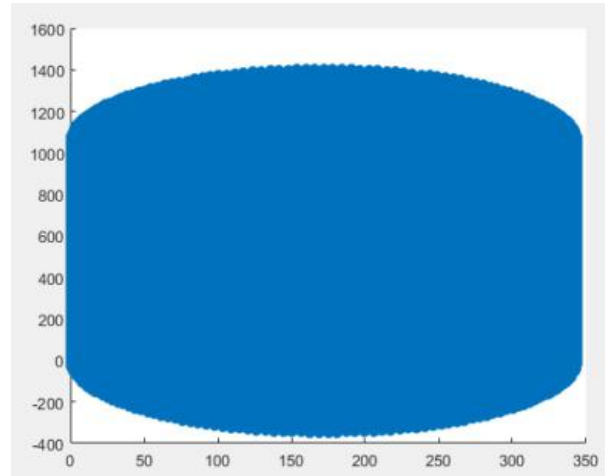


Figure4. Ground Scanning Area Simulation

3.3 Improvement of Pulse Emission Waveform of Laser

In order to improve the scanning accuracy, it is necessary to increase the density of scanning points. In this paper, the laser pulse emission waveform is improved to realize the interpolation between two scanning corners and to enhance the scanning point density. The circle of static scanning is divided into upper half circle and lower half circle. There are 88 points in the first half and the second half. The eighty-eighth point is the last point in the first half, and the eighty-ninth point is the last point in the second half. The eighty-eighth point and the eighty-ninth point delay $1/5500 \times 3/2$ seconds. The seventeenth point and the first point in the next circle need to be delayed $1/5500 \times 1/2$ seconds. As shown in Figure 3.2, the scanning density is increased. Figure 5 Local scan results.

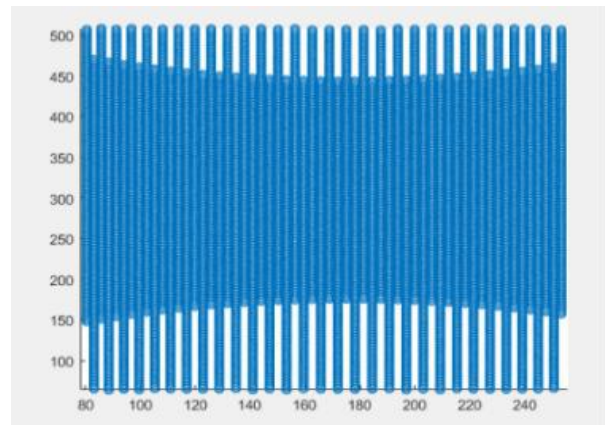


Figure 5. Local scan results

3.4 Comparison of Double Wedge and Single Wedge

Double optical wedge is an optical system composed of two optical wedge working faces. Formula 6 is a single wedge calculation formula. The advantage of double wedges is that large deflection angle can be obtained by using small wedge angle. The deflection angle is calculated as formula 5

$$n \sin(\arcsin(\frac{\theta+\alpha}{n}) - \alpha) = \sin\alpha$$

(5)

The optical wedge used in this paper is a single optical wedge, because the deflection angle is only 10 degrees, the very small wedge angle brings inconvenience to the processing.

Fig 6 is a diagram of double optical wedges.

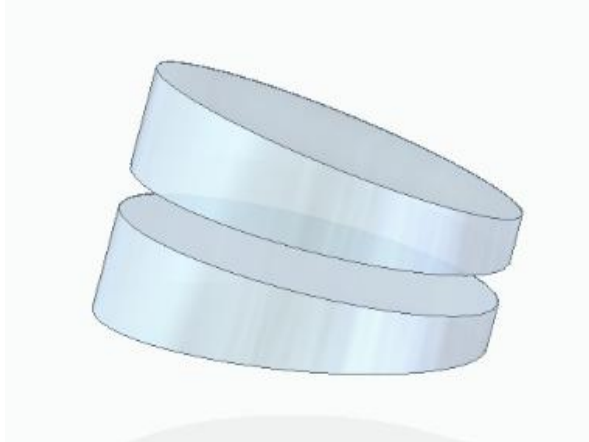


Figure 6. Diagram of double optical wedges

3.5 Design Of Optical Wedge

A wedge is a refractive prism with the ability to deflect light. The working surface of refractive prism is two refractive surfaces. Two refractive surfaces. The intersection line of two refraction surfaces is called refraction edge, and the dihedral angle between two refraction surfaces is called refraction prism angle. Similarly, the plane perpendicular to the refractive prism is called the main section of the refractive prism.

When a prism with a small refraction angle is called a wedge, the formula of its deflection angle can be greatly simplified because of its small refraction angle. When I_1 is of finite size, it can be regarded as a parallel plate because of its small angle. There is a formula 6.

$$\delta = n(\frac{\cos I_1'}{\cos I_1} - 1)\alpha$$

(6)

When I_1 is very small, there is a formula (7) for I_1' , where the refractive prism is a wedge. Fig 7 is a diagram of a wedge.

$$\delta = (n - 1)\alpha$$

(7)

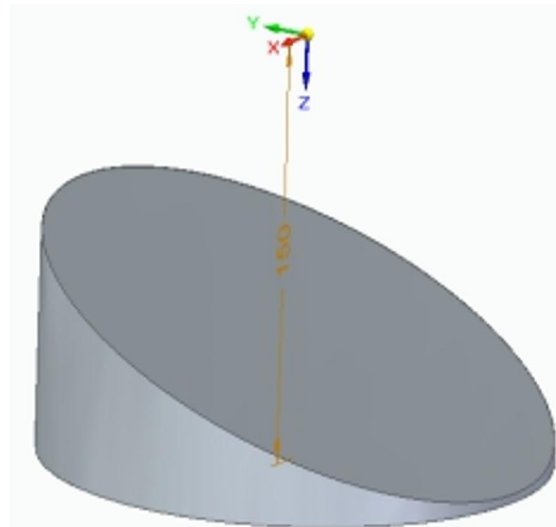


Figure 7. Diagram of optical wedge

$\tan \theta = 0.175$ is calculated from formula 4. The inverse solution gives $\theta=9.93$ degrees. In order to meet the requirement of better generality of other wavelength lasers, N-FK58 material is chosen in this paper. It is a kind of ultra-high dispersion material. Its performance is as shown in Table 3. Table 3 N-FK58 Material Properties

parameter	value
optical material	N-FK58
abbe number	90.90
Laser damage threshold	2J/cm^2
Transmissivity	0.998
Refractive index	1.44998 (1064nm)

Table 3. N-FK58 Material Properties

According to formula 6, the wedge angle of optical wedge is 22.07 degrees, the minimum lens thickness is 3 mm, and the maximum lens thickness is 84.09 mm.

3.6 Compensating lens

In order to eliminate dispersion, the optical system still needs to add compensating lens to reduce dispersion. We use Zemax software for analysis.

The design criteria of compensating lens are as follows: double glued lens is used to eliminate dispersion, and its image space F number is 10, 5-degree half field of view is selected, and the sampling points are 0, 3.5 and 5, respectively.

As shown in Figure 8, after the compensating lens, the 1064nm and 532nm light basically coincide.

Fig 9 is the 3-D layout of the lens.

The conclusion is that two materials, N-PSK58 and LASF18A, should be used.

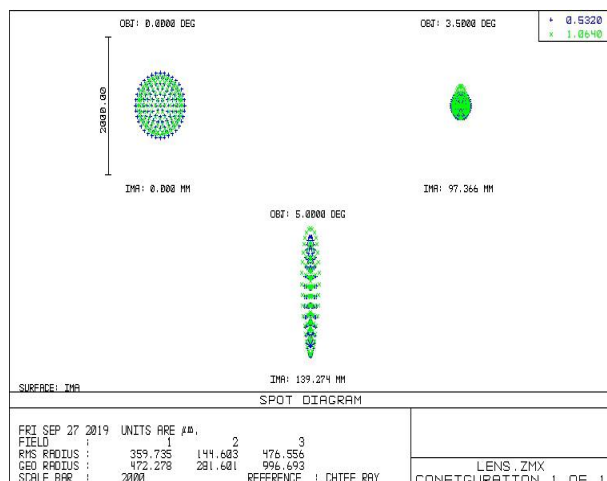


Figure 8. IMA Diagram of Compensation Lens

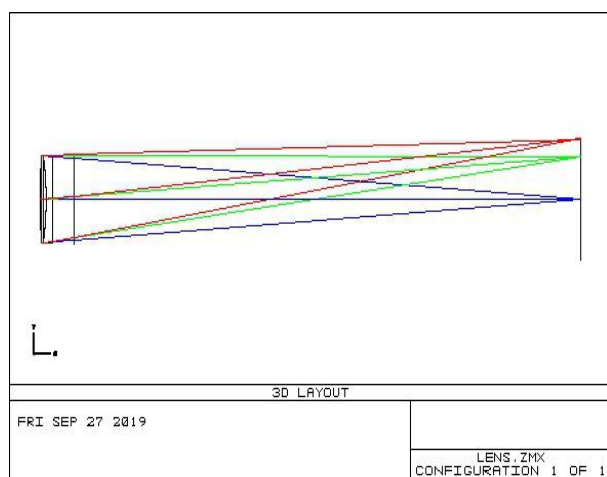


Figure 9. 3-D layout of lens

3.7 Parameter Design of Control Motor

The speed of the motor is the scanning frequency. The scanning angle point N, the laser pulse repetition frequency F and the scanning frequency relation f are as follows: Formula 8.

$$N = \frac{F}{f} \quad (8)$$

Take the data into the operation and get $f = 31.25$. The speed of the hollow motor should be 31.25 rpm. The total weight of airborne LiDAR should not be too large, so the purchased motor should be within 10 kg. The core component of the control circuit is the chip. Its circuit schematic diagram is shown in Figure 10

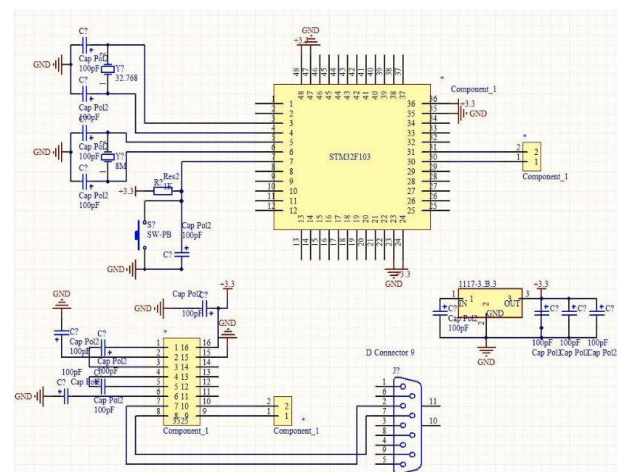


Figure 10. The circuit principle diagram

4. CONCLUSION

The single laser point LiDAR will remain the mainstream LiDAR in the next 10 years. The LiDAR scanner designed in this paper improves the laser pulse waveform, improves the scanning accuracy, and the overall size of the scanner is small enough to be loaded on small aircraft. The scanner still has some shortcomings.

- (1) The scanning accuracy of LiDAR is affected by the changes of altitude, speed and attitude angle during the flight. The scanner has no control system and cannot adjust the flight state of the aircraft.
- (2) The lens of optical wedge belongs to the precision equipment. The environment on the plane is shaking violently and needs regular cleaning and maintenance. The reliability is poor.
- (3) There are almost no ultra-high-speed hollow motors in the domestic market, so it is very difficult.
- (4) Final effect diagram is Fig11

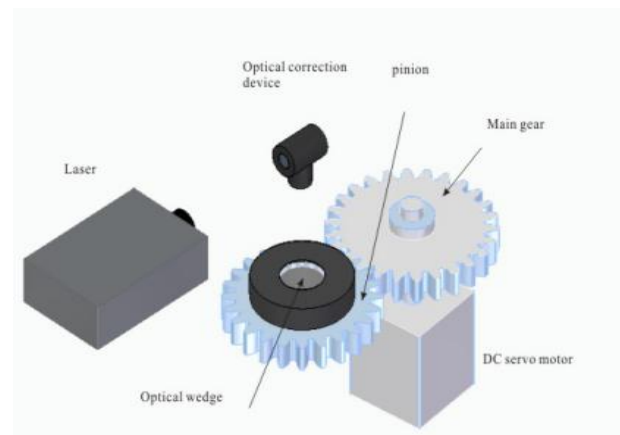


Figure 11. all of system diagram

ACKNOWLEDGMENTS

This paper is financially supported by the National Natural Science of China under Grant numbers 41431179, 41961065; Guangxi Innovative Development Grand Grant under the grant number: GuikeAA18118038, GuikeAA18242048; the National Key Research and Development Program of China under Grant numbers 2016YFB0502501 and the BaGuiScholars program of Guangxi (Guoqing Zhou)

REFERENCES

- Aaron G. Kamoske. 2019. Leaf area density from airborne LiDAR: Comparing sensors and resolutions in a temperate broadleaf forest ecosystem. *Forest Ecology and Management*:364-375.
- Ahmed Shaker. 2019. Automatic land-water classification using multispectral airborne LiDAR data for near-shore and river environments. *ISPRS Journal of photogrammetry and Remote Sensing*:94-108.
- Adam J. Mathews. 2019. Satellite scatterometer estimation of urban built-up volume: Validation with airborne LiDAR data. *International Journal of Applied Earth Observations and Geoinformation*:100-107.
- Conllins B. Kukunda. 2019. Scale-guided mapping of forest stand structural heterogeneity from airborne LiDAR. *Ecological Indicators*:410-425.
- Cheng Y. ,2019, Hierarchical tunnel modeling from 3D raw LiDAR point cloud. *Computer-Aided Design*:143-154.
- Dong-Cheon Lee. 2019. Determination of Building Model Key Points Using Multidirectional Shaded Relief Images Generated from Airborne Data. *Journal of Sensors*:15-20.
- Feigels V I, Gilbert G D., 1992, SPIE Proceedings [SPIE San Diego '92 - San Diego, CA (Sunday 19 July 1992)] Ocean Optics XI. 1750:473-484.
- Hu T. ,2019, A simple and integrated approach for fire severity assessment using bi-temporal airborne LiDAR data. *International Journal of Applied Earth Observations and Geoinformation*:25-38.
- J. Degerickx., 2019, Enhancing the performance of MESMA for urban land cover mapping using airborne LiDAR data and band selection. *Remote Sensing of Environment*:206-273.
- Li K., Zhang Y. Liu X., et al .,2015, Study on receiving FOV in airborne laser ocean sounding system. *Acta Optica Sinica*, 35(7).
- R. L Shrestha. ,2005, Airborne Laser Swath Mapping: Quantifying changes in sandy beaches over time scales of weeks to years *ISPRS Journal of photogrammetry and Remote Sensing*:222-232.
- Sakitt B. Indices of discriminability., 1973, *Nature*, 241(5385): 133-134.
- Wang L. 2013, Error Processing Theory and Method of Airborne LiDAR Data Error Processing. *Surveying and Mapping Publishing House*:18-20.
- Zhou. G, Huang J. and Zhang. G, 2015. Evaluation of the wave energy conditions along the coastal waters of Beibu Gulf, China, *Energy*, vol. 85, pp. 449–457.
- Zhou. G, Zhou X, Yang J, Yue Tao, Nong X.,2015, Oktay Baysal, Flash Lidar Sensor using Fiber Coupled APDs, *IEEE Sensor Journal*, vol. 15, no. 9, September, pp. 4758-4768.
- Zhou G., L. Huang J., Zhang R., Liu D., Zhou X. and O. Baysal, FPGA-based on-board geometric calibration for linear CCD imager, *Sensors*, 18, 1794; doi:10.3390/s18061794, 2018.
- Zhou G., Yang J. Z., Yu X., and Zhu W., "Power supply topologyfor LiDAR system onboard UAV platform," Proc. SPIE, vol. 8286, pp. 828606-1–828606-6, Oct. 2011.